THE JOURNAL OF PHYSICAL CHEMISTRY C
A JOURNAL OF THE AMERICAN CHEMICAL SOCIETY

pubs.acs.org/JPCC

Article

Syngas Conversion on the Different Cu Surfaces: The Relationship of the Coordination Number of Cu Active Sites with the Activity and Selectivity of Key Intermediate CH_x Production

Wantong Zhao, Lixuan Ma, Baojun Wang,* Lixia Ling, and Riguang Zhang*

Cite This: *J. Phys. Chem. C* 2021, 125, 23085−23097

Read Online

ACCESS | Metrics & More | Article Recommendations | Supporting Information

ABSTRACT: Aiming at exploring the relationship of the Cu generalized coordination number (GCN) with the activity and selectivity of CH_x (x = 1−3) and CH_3OH from syngas on the Cu catalyst, DFT calculations and microkinetic modeling were used to clarify the mechanism of syngas conversion on different Cu surfaces with the GCNs of 4, 4.7, 5.5, 6.5, and 7.5, respectively. The results show that the GCNs of Cu active sites impact the optimal path of CH_x (x = 1−3) and CH_3OH production, change the existing form of primary CH_x monomers, and alter the corresponding selectivity and yield. Among these Cu catalysts, the 4.7-GCN of Cu active sites exhibits the highest activity toward the production of primary CH_2 monomers and CH_3OH; however, the activity of CH_3OH production is higher than that of CH_2, leading to a low CH_2 selectivity. Both 5.5-GCN and 6.5-GCN of Cu active sites exhibit moderate activity of CH_2 production and significantly low activity of CH_3OH production; thus, the 5.5-GCN and 6.5-GCN of Cu active sites present the highest selectivity toward primary CH_2 monomers and effectively inhibit CH_3OH production. This study offers valuable clues for the design of other metal catalysts with excellent catalytic performance toward CH_x (x = 1−3) production by adjusting the GCNs of active sites.

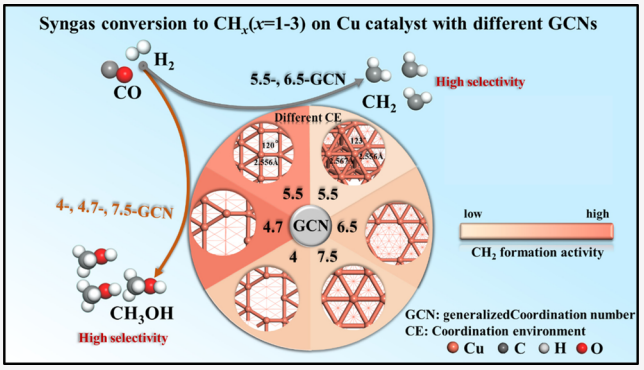

1. INTRODUCTION

Nowadays, the major challenge for C_2 oxygenate production from syngas (CO and H_2) is low yield and selectivity,[1,2] even if it is strongly exothermic.[3,4] Rh catalysts are promising to present high C_2 oxygenate selectivity from syngas at 250−320 °C with the pressures of 1−30 bar;[5−8] however, low CO conversion, low yield of C_2 oxygenates, and high cost limit their industrial application. Nowadays, Cu catalysts have been widely applied in the industrial methanol synthesis via the hydrogenation of CO or CO_2; for example, Behrens et al.[9] proposed that the $Cu/ZnO/Al_2O_3$ catalyst exhibits high activity toward the hydrogenation of CO or CO_2 to produce CH_3OH, which is attributed to the enhanced binding ability of the intermediates and the decreased energy barrier of CH_3OH production. Kattel et al.[10] found that the synergistic effect of Cu and ZnO nanoparticles promotes CH_3OH production via the hydrogenation of CO_2. Grabow et al.[11] proposed that the oxidized Cu(110), (100), and (211) surfaces provide active sites to facilitate CH_3OH production. Compared to Rh, the low cost Cu has high CO conversion at 280−310 °C with the pressure range of 40−100 bar;[12,13] however, methanol is easily produced, resulting in the low selectivity and yield of C_2 oxygenates. Thus, the Cu catalyst for CH_3OH production by the hydrogenation of CO and CO_2 is expected to be modified in this study and further alter product selectivity toward higher alcohols.

Generally, the accepted mechanism for C_2 oxygenate production from syngas on the Cu catalyst includes two critical steps;[1,2,14−17] the first is the production of key intermediates CH_x (x = 1−3); after this, CO/CHO inserts into CH_x to form $CH_xC(H)O$ as the precursor of C_2 oxygenates and, subsequently, its continuous hydrogenation to form C_2 oxygenates. Moreover, once the intermediates CH_x (x = 1−3) are produced, the Cu catalyst prefers the production of C_2 oxygenates via CO/CHO insertion into CH_x,[18−20] thus aiming at enhancing the selectivity and yield of C_2 oxygenates on the Cu catalyst; how to boost the production of CH_x (x = 1−3) intermediates becomes a matter of urgency, which is the key step in the production process of C_2 oxygenates from syngas. Furthermore, for the production of CH_x (x = 1−3) intermediates from syngas,[19−21] it includes two ways: one is

Received: May 30, 2021
Revised: September 25, 2021
Published: October 19, 2021

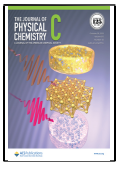

https://doi.org/10.1021/acs.jpcc.1c04763
J. Phys. Chem. C 2021, 125, 23085−23097

the direct dissociation of CO into C and, subsequently, its successive hydrogenation to form CH_x; the other is hydrogen-assisted dissociation of CO to form CH_xO or CH_xOH and, subsequently, its C−O(H) bond breakage to produce CH_x; alternatively, the successive hydrogenation of CH_xO or CH_xOH produces methanol, which decreases CH_x selectivity and yield. The product selectivity in syngas conversion strongly depends on the ability of C−O bond scission in CO or CH_xO/CH_xOH intermediates from CO hydrogenation. For example, Medford et al.[4] fully studied the production of C_{2+} oxygenates from syngas on the different transition metal M(211) (M = Rh, Ru, Ni, Ir, Pd, Pt, Cu, Au, Ag) surfaces, suggesting that the C−O bond scission is difficult on the Cu, Au, and Ag surfaces; the main product is methanol; however, the C−O bond scission easily occurs on the Ru, Rh, Ni, Ir, Pd, and Pt surfaces, and the main product is methane. Interestingly, Mei et al.[7] found that the ability of C−O bond scission is moderate on Mn-doped Rh catalysts, C_{2+} oxygenates become the dominant product since the dissociated CO can provide CH_x intermediates, and the undissociated CO inserts into CH_x to produce C_2 oxygenate precursors. Furthermore, Schumann et al.[22] analyze the selectivity of C_{2+} oxygenates from syngas on the fcc transition metal M(111) (M = Rh, Co, Pd, Pt, Cu, Ag) catalysts, indicating that the easy C−O bond scission in CO or CH_xO/CH_xOH intermediates leads to methane production on the Rh and Co, whereas the C−O bond scission of CO or CH_xO/CH_xOH is hard, which results in methanol production on the Pd, Pt, Ag, and Cu. Furthermore, Studt et al.[23] proposed that methanol is the main product on the Cu catalyst due to the difficult C−O bond scission. Liu et al.[24] found that the C−O bond scission easily occurs on the Co catalyst, and the main product is C_{2+} hydrocarbons. Thus, aiming at promoting CH_x (x = 1−3) production on the Cu catalyst, methanol formation must be inhibited.

Previous studies reported that changing the coordination number (CN) of active sites on the catalyst can effectively improve their catalytic performance toward the targeted reactions.[25−29] For example, Gao et al.[30] fully researched the hydrogen evolution reaction (HER) and oxygen evolution reaction (OER) on the graphene anchored Ni catalysts; the Ni active site with 1-CN shows the highest activity for the HER compared with that with 2-, 3-, and 4-CN, while the Ni active site with 4-CN shows the highest activity for the OER. Jiang et al.[31] found that the spillover hydrogenation only happens on 8-CN Pd_1/Cu(100) rather than that on 9-CN Pd_1/Cu(111), which is preferable for alkyne semihydrogenation. Xu et al.[32] discovered that highly coordinated Pt single atoms enhanced propylene selectivity in propane semihydrogenation.

Meanwhile, the vacancy can change the CN of active sites on the catalyst surface and improve the catalytic performance. Xie et al.[33] reported that the point defects and atom vacancies could result in the enrichment of coordinately unsaturated atoms to improve HER activity. Kopač et al.[34] found that the stepped Cu(553) surface with 7-CN of Cu active sites shows high activity and selectivity toward methanol compared to the Cu(111) surface with 9-CN of Cu active sites. Chen et al.[35] discovered that molybdenum sulfide with 2S vacancies promoted CO conversion into CH_4 with excellent selectivity and activity. The monovacancy graphene-supported metal atoms favored O_2 dissociation compared to the double-vacancy graphene.[36] Zhuang et al.[37] showed that the selectivity of liquid alcohols increased in CO_2 electrochemical reduction on the S-enriched Cu vacancy surface with 8-CN Cu active sites compared with that on the 9-CN Cu active sites. Furthermore, the defective crystal surfaces could exist stably; for example, Behrens et al.[9] prepared the Cu/ZnO/Al_2O_3 industrial catalyst and found that the presence of steps results in high activity toward methanol production on Cu/ZnO/Al_2O_3; more importantly, the steps can be stabilized by bulk defects such as stacking faults or twin boundaries. Gu et al.[38] utilized a CO-rich environment to synthesize a defect-rich Cu catalyst, which shows excellent stability during a continuous 30 h operation of electrochemical CO_2 reduction. Rong et al.[39] utilized the precursors including both nitrogen and oxygen atoms to remove the oxygen atom of Ni−N_3O below 800 °C, and a vacancy-defect Ni−N_3−V is generated, which exhibits long time stability and retains 95% of the initial current density after 14 h electrolysis.

Based on the above analysis, the vacancy introduced into the catalyst surface can adjust the CNs of active sites to improve its catalytic performance. However, up to now, the relationship of the CNs of Cu active sites with the activity and selectivity of key intermediate CH_x (x = 1−3) production from syngas on the Cu catalyst is still unclear.

Aiming to illustrate the above issues, this study was designed to examine the key steps including the activation of CO and the CH_x (x = 1−3) intermediate production in syngas conversion on Cu catalysts with different CNs of Cu active sites. Here, DFT calculations and microkinetic modeling are adopted. Furthermore, the d-band center of surface Cu atoms around the vacancy, differential charge density, and Mulliken charge are analyzed to reveal the relationship between the CNs of Cu active sites and the catalytic performance. The valuable structure clues according to CNs of active sites are offered for the rational construction of Cu catalysts with excellent catalytic activity and selectivity toward CH_x (x = 1−3) intermediate production from syngas.

2. COMPUTATIONAL DETAILS

2.1. Calculation Methods. All theoretical calculations were conducted by DFT using the Dmol^3 code of Materials Studio 8.0. The electronic exchange-correlation functions were adopted for the generalized gradient approximation[40] with the Perdew−Burke−Ernzerhof.[41] An effective core potential was implemented to treat the inner electrons of Cu atoms.[42] The valence electron wave functions were treated by the double numerical basis plus polarization.[43−45] A 3 × 3 × 1 k-point grid of the surface Brillouin zone was used, and a Methfessel-Paxton smearing is set to 0.005 Ha.[46] The geometry optimization with convergence criteria of energy, displacement, and force correspond to 2.0 × 10^{-5} Ha, 0.005 Å, and 0.004 Ha/Å, respectively. The convergence criterion of SCF (self-consistent field) is 1.0 × 10^{-5} Ha.

The transition states of elementary reactions included in the production of CH_x (x = 1−3) and CH_3OH were located using the Complete LST/QST method.[47,48] The transition state was verified by TS Confirmation and frequency analysis.

2.2. Surface Models. The catalytic reaction usually occurs at the metal defects under the realistic conditions in which the structure and electronic properties of active sites are changed to improve catalytic performance.[49] In essence, this phenomenon is attributed to the CN change of active sites caused by the defects.[50] Furthermore, the type or the number of vacancies could lead to different CNs of active sites.[51,52]

Aiming at exploring the relationship between Cu catalysts with different CNs of Cu active sites and the catalytic

https://doi.org/10.1021/acs.jpcc.1c04763
J. Phys. Chem. C 2021, 125, 23085−23097

performance of CH_x (x = 1−3) intermediate production from syngas, Cu catalysts with the CN of Cu active sites ranging from 9-CN to 6-CN are constructed. The reason for constructing CNs ranging from 9-CN to 6-CN is mainly based on the previous studies by Grunwaldt et al.,[53] which suggests that the CN of Cu active sites has obviously changed from 5 to 6.9 and 6.3 after three "dry" syngas recycles on the Cu/ZnO catalyst; however, the CN of Cu active sites has obviously changed from 8.3 to 8.8 and 7.7 after three "wet" syngas recycles.

Cu(111) is the most stable and mainly exposed surface of the Cu catalyst;[5] thus, as presented in Figure 1, the

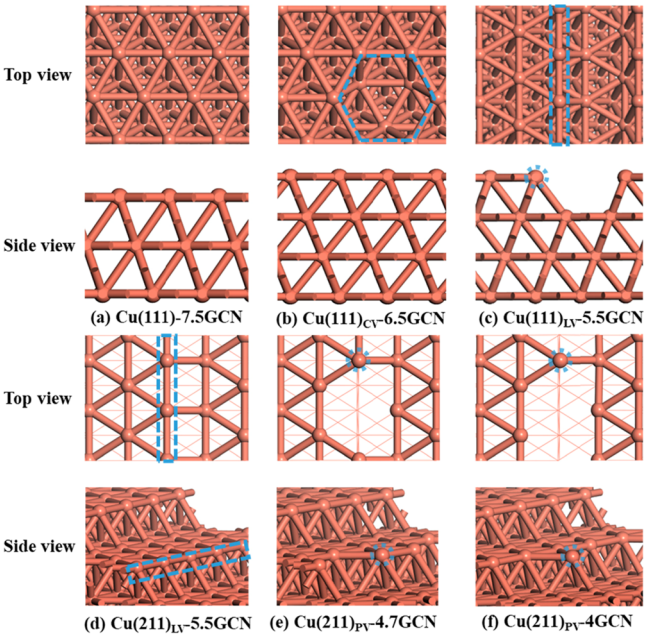

Figure 1. Top and side views for surface models of (a) Cu(111)-7.5GCN, (b) $Cu(111)_{CV}$-6.5GCN, (c) $Cu(111)_{LV}$-5.5GCN, (d) $Cu(211_{)LV}$-5.5GCN, (e) $Cu(211)_{PV}$-4.7GCN, and (f) $Cu(211)_{PV}$-4GCN. The region marked in bright blue indicates the active site of the surface.

comparisons between the Cu(111) surface and other defective surfaces are carried out to illustrate the effect of Cu defect type on the catalytic performance. Usually, the CN of Cu active sites indicates the number of Cu atoms linked with the nearest neighboring atoms, so the surface Cu atom on Cu(111) corresponds to the 9-CN Cu active site, denoted as Cu(111)-9CN; then, a Cu atom and a line of Cu atoms are removed from the Cu(111) surface to obtain the circle and line vacancies, respectively, which lead to 8-CN and 7-CN Cu active sites, named as $Cu(111)_{CV}$-8CN and $Cu(111)_{LV}$-7CN. On the other hand, the step is the most common defect on the metal catalyst surface,[20] and the Cu(211) surface with the (100)-type step can well present the structural characteristic of the step defect with 7-CN Cu active sites,[54] denoted as $Cu(211)_{LV}$-7CN; then, a Cu atom is removed from the stepped edge of Cu(211) to form the point vacancy with the 6-CN Cu active site, denoted as $Cu(211)_{PV}$-6CN; furthermore, a Cu atom at the stepped edge near the 6-CN Cu active site is removed to form the point vacancy with the 5-CN Cu active site, denoted as $Cu(211)_{PV}$-5CN.

In recent years, the generalized coordination number (GCN) of the surface active sites including the first and second nearest neighbors is used to reflect the surface properties, which can provide more accurate descriptions than the usual CN to understand the chemical reactivity of the pure metals.[55−57] For example, Calle-Vallejo et al.[55] proposed that GCNs of the active sites can quickly and accurately guide the selection of the excellent catalyst in experiment, indicating that the Pt catalyst with the 8.3-GCN active site has the highest activity toward the oxygen reduction reaction (ORR), which is verified by experiments; moreover, the Pt catalyst with 8.3-GCN show a higher catalytic activity than Pt(111) with 7.5-GCN. Thus, the GCNs of Cu active sites are used in this study and obtained by the following equation:[58]

$$\mathrm{GCN(i)} = \sum_{j=1}^{n_i} \frac{\mathrm{CN(j)}}{\mathrm{CN_{max}}} \quad (1)$$

where j represents the first nearest neighbor of Cu active site i, and CN(j) represents the CN of site j. CN_{max} represents the maximum CN in Cu bulk. As listed in Table S1, the GCN of the Cu active site on Cu(111) is 7.5, and thus, Cu(111)-9CN is denoted as Cu(111)-7.5GCN; then, the GCNs of the Cu active site on $Cu(111)_{CV}$-8CN, $Cu(111)_{LV}$-7CN, $Cu(211)_{LV}$-7CN, $Cu(211)_{PV}$-6CN, and $Cu(211)_{PV}$-5CN are 6.5, 5.5, 5.5, 4.7, and 4, denoted as $Cu(111)_{CV}$-6.5GCN, $Cu(111)_{LV}$-5.5GCN, $Cu(211)_{LV}$-5.5GCN, $Cu(211)_{PV}$-4.7GCN, and $Cu(211)_{PV}$-4GCN, respectively. Cu(111)-7.5GCN is modeled using a three-layer $p(3 \times 3)$ unit cell, where the adsorbates and the upper two layers are relaxed, and the bottom one layer is fixed. $Cu(111)_{PV}$-6.5GCN and $Cu(111)_{LV}$-5.5GCN are constructed using a four-layer $p(4 \times 4)$ unit cell, where the adsorbates and the upper three layers are relaxed, and the bottom one layer is fixed in which the $p(3 \times 3)$ unit cell with vacancies is too small to react. $Cu(211)_{LV}$-5.5GCN, $Cu(211)_{PV}$-4.7GCN, and $Cu(211)_{PV}$-4GCN are constructed using an eight-layer $p(2 \times 3)$ unit cell,[20] where the adsorbates and the upper five layers are relaxed, and the bottom three layers are fixed. A 15 Å vacuum thickness is to eliminate the layer-to-layer interaction.

3. RESULTS AND DISCUSSION

3.1. Production Path of CH_x and CH_3OH on the Cu Catalyst. As mentioned in the Introduction section, the production of key CH_x (x = 1−3) intermediates from syngas[59−61] includes two possible ways: one way is the direct dissociation of CO into C and O and, subsequently, its continuous hydrogenation to form CH_x; the other way is hydrogen-assisted dissociation of CO to form CH_xO/CH_xOH, and subsequently, CH_x is produced via the C−O(H) bond breakage of CH_xO/CH_xOH; alternatively, the hydrogenation of CH_xO or CH_xOH can produce methanol, which decreases the yield and selectivity of CH_x. Thus, the possible production paths of CH_x (x = 1−3) and methanol from syngas on the Cu catalyst are presented in Figure 2. Since syngas conversion to CH_x (x = 1−3) and CH_3OH usually happens at 500−623 K,[1,3,12,62] the activation free energy (ΔG_a) and reaction free energy (ΔG) at 523 K and under the standard pressure of all elementary reactions included in the production of CH_x (x = 1−3) and CH_3OH on Cu catalysts with different GCNs of Cu active sites are listed in Table S3.

3.2. Adsorption of the Species on the Cu Catalyst with Different GCNs of Cu Active Sites. The adsorption energies and the most stable adsorption configurations of CO, CHO, CHOH, CH_2O, CH_3O, and CH_2OH species on

https://doi.org/10.1021/acs.jpcc.1c04763
J. Phys. Chem. C 2021, 125, 23085−23097

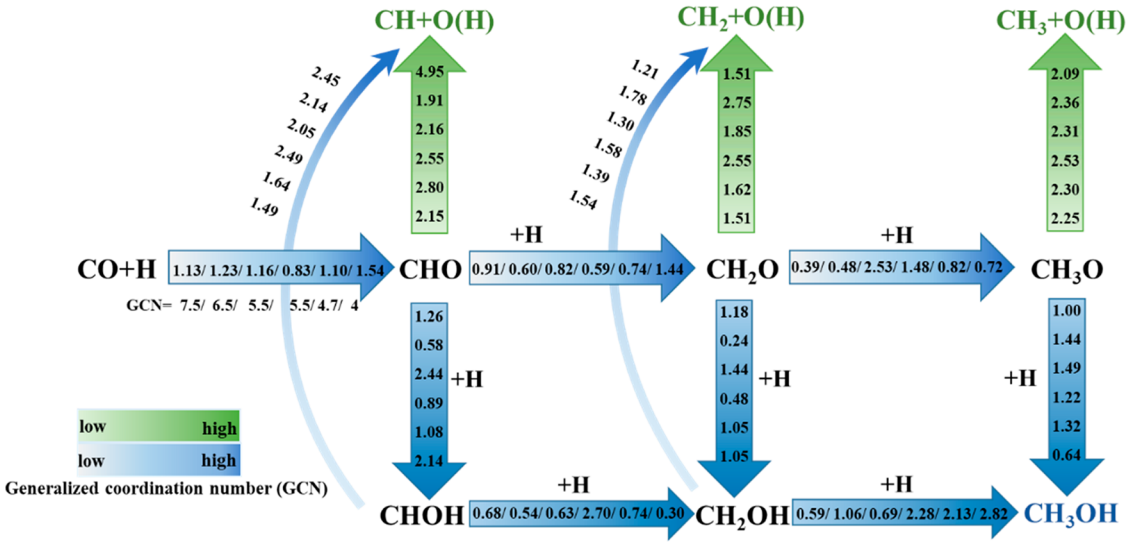

Figure 2. Reaction network of CH_x (x = 1−3) intermediates and methanol production from syngas on the Cu catalyst with different generalized coordination numbers. The values are the activation free energy of the elementary reaction involved in the CH_x (x = 1−3) intermediate and methanol production from syngas.

Cu(111)-7.5GCN, $Cu(111)_{CV}$-6.5GCN, $Cu(111)_{LV}$-5.5GCN, $Cu(211)_{LV}$-5.5GCN, $Cu(211)_{PV}$-4.7GCN, and $Cu(211)_{PV}$-4GCN are listed in Table S2 and Figure S1.

As presented in Figure 3a,b, the adsorption energies of CO, CH_2O, and CH_3O decrease with decreasing GCNs of Cu active sites, while those of CHO, CHOH, and CH_2OH first decrease and then increase. In general, compared to Cu(111)-7.5GCN, the adsorption ability of CO, CHO, CH_2O, CH_3O, CHOH, and CH_2OH increases on $Cu(111)_{CV}$-6.5GCN, $Cu(111)_{LV}$-5.5GCN, $Cu(211)_{LV}$-5.5GCN, $Cu(211)_{PV}$-4.7GCN, and $Cu(211)_{PV}$-4GCN. Furthermore, Tafreshi et al.[64] also discovered that the hydrazine adsorption energy on the 7-CN Cu(110) surface is much stronger than that of the 8-CN Cu(100) and 9-CN Cu(111) surfaces, suggesting that the CNs of Cu active sites significantly impact the adsorption ability of the correlative species.

3.3. CO Initial Activation. CO initial activation exits two ways: the direct dissociation of CO and the hydrogenation of CO to form CHO/COH, as shown in Figure 4; the activation free energies of CO direct dissociation and its hydrogenation to COH are much higher than those of CHO formation on Cu catalysts with different GCNs of Cu active sites, suggesting that the initial activation of CO is advantageous to form CHO rather than COH, which are consistent with the previously reported results. For example, DFT studies[1] found that CO activation primarily occurs via H-assisted dissociation to produce CHO on the Cu(111) surface. Zhang et al.[20] showed that the Cu(211) surface is detrimental to the direct dissociation of CO into C and O; meanwhile, CO is activated mainly via the hydrogenation to form CHO.

The activation free energy of CHO formation is in the sequence $Cu(211)_{PV}$-4GCN > $Cu(111)_{CV}$-6.5GCN > $Cu(111)_{LV}$-5.5GCN > Cu(111)-7.5GCN ≈ $Cu(211)_{PV}$-4.7GCN > $Cu(211)_{LV}$-5.5GCN (1.54, 1.23, 1.16, 1.13, 1.10, and 0.83 eV), and the reaction free energies are 0.76, 0.57, 0.35, 0.77, 0.53, and 0.52 eV, respectively, suggesting that the GCNs of Cu active sites impact the reactivity of CO activation; especially, $Cu(211)_{LV}$-5.5GCN has the highest activity compared to the other catalysts.

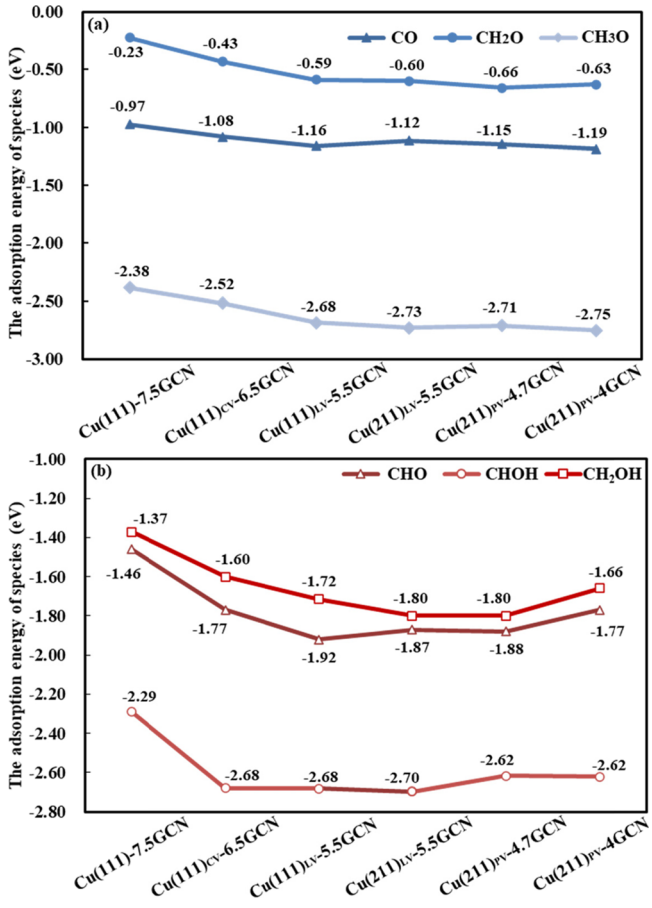

Figure 3. Adsorption energy (E_{ads}/kJ·mol^{-1}) of (a) CO, CH_2O, and CH_3O and (b) CHO, CHOH, and CH_2OH on Cu(111)-7.5GCN, $Cu(111)_{CV}$-6.5GCN, $Cu(111)_{LV}$-5.5GCN, $Cu(211)_{LV}$-5.5GCN, $Cu(211)_{PV}$-4.7GCN, and $Cu(211)_{PV}$-4GCN.

Furthermore, both $Cu(111)_{LV}$-5.5GCN and $Cu(211)_{LV}$-5.5GCN have the same GCNs of Cu active sites; however, $Cu(211)_{LV}$-5.5GCN shows a much higher activity toward CO activation than $Cu(111)_{LV}$-5.5GCN, which is attributed to the

https://doi.org/10.1021/acs.jpcc.1c04763
J. Phys. Chem. C 2021, 125, 23085−23097

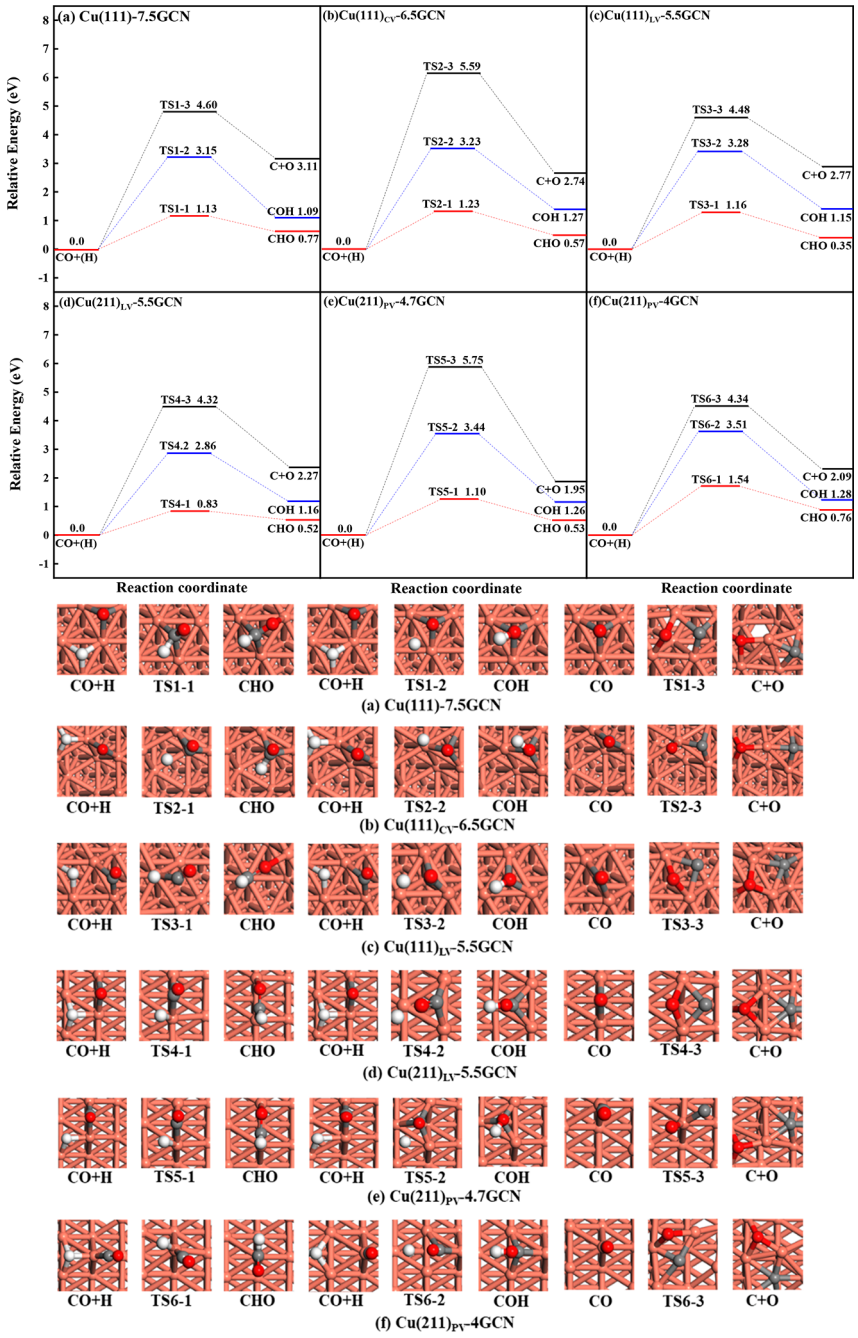

Figure 4. Potential energy profile of CO initial activation from syngas with the structures of initial states, transition states, and final states on (a) Cu(111)-7.5GCN, (b) $Cu(111)_{CV}$-6.5GCN, (c) $Cu(111)_{LV}$-5.5GCN, (d) $Cu211_{)LV}$-5.5GCN, (e) $Cu(211)_{PV}$-4.7GCN, and (f) $Cu(211)_{PV}$-4GCN. Orange, Gray, red, and white balls represent Cu, C, O, and H atoms, respectively.

different B_5 active site. As shown in Figure 5a,b, the angle of Cu−Cu−Cu is 123° on $Cu(111)_{LV}$-5.5GCN, while that of $Cu(211)_{LV}$-5.5GCN is 120°; the Cu−Cu bond lengths of the B_5 active site are all 2.556 Å on $Cu(211)_{LV}$-5.5GCN; however, those of $Cu(111)_{LV}$-5.5GCN are 2.565, 2.533, 2.567, and 2.556 Å, respectively, which change the stability of the transition state for CO hydrogenation to CHO and further affect its activation ability. As shown in Figure 5c, the adsorption energy of the initial state (CO + H) on $Cu(111)_{LV}$-5.5GCN (−3.59 eV) is nearly the same as that of $Cu(211)_{LV}$-5.5GCN (−3.61 eV). However, the adsorption ability of the transition state on $Cu(211)_{LV}$-5.5GCN (−2.76 eV) is stronger than that of $Cu(111)_{LV}$-5.5GCN (−2.44 eV); that is, $Cu(211)_{LV}$-5.5GCN can stabilize the transition state of CO hydrogenation to CHO and presents high activity compared to $Cu(111)_{LV}$-5.5GCN; the reasons may be that the B_5 active sites result in a weaker repulsion between CO and H atoms on $Cu(211)_{LV}$-5.5GCN (∠H−Cu−C = 46.5°) compared to those on $Cu(111)_{LV}$-5.5GCN (∠H−Cu−C = 47.3°).

3.4. Production of CH_x Intermediates and Methanol.

As discussed above, CO initial activation dominantly form CHO on Cu catalysts; thus, CH_x (x = 1−3) intermediates are produced via the dissociation of CH_xOH (x = 1,2) and CH_xO (x = 1−3) formed by CHO hydrogenation.

3.4.1. CH Production. For CH production, there are two paths: one is CO + H → CHO → CH + O; the other is CO +

https://doi.org/10.1021/acs.jpcc.1c04763
J. Phys. Chem. C 2021, 125, 23085−23097

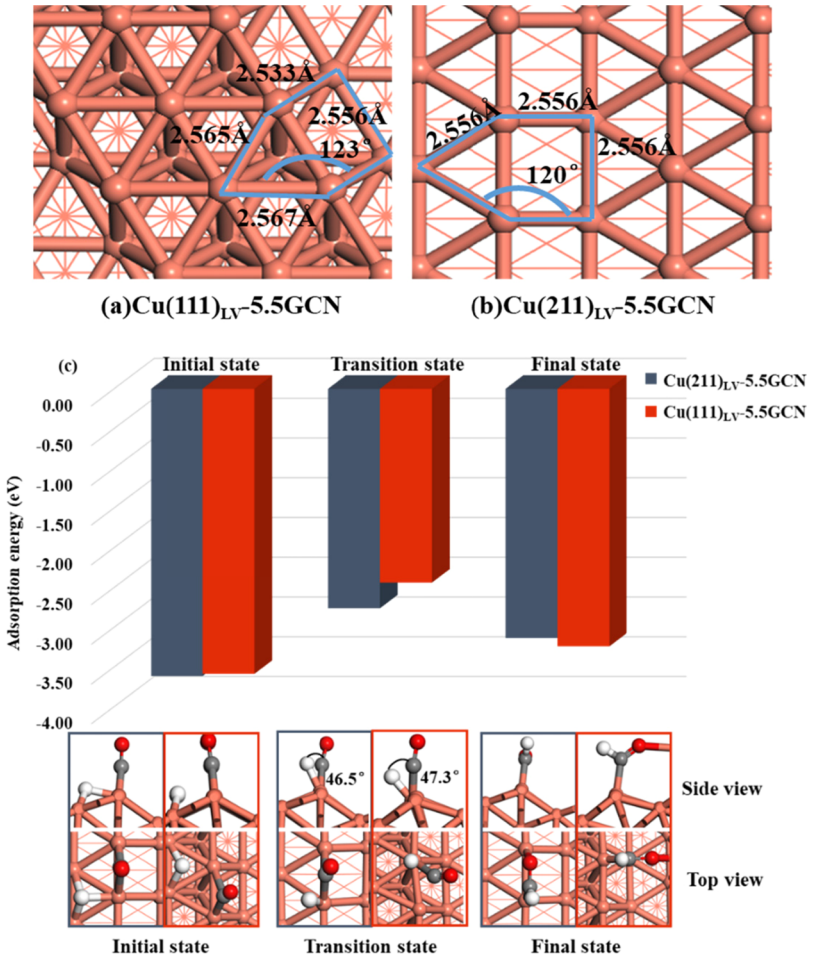

Figure 5. Coordination environment of B_5 active sites on (a) $Cu(111_{)LV}$-5.5GCN and (b) $Cu(211_{)LV}$-5.5GCN; (c) adsorption energies and configurations of the initial and the transition and final states on $Cu(111_{)LV}$-5.5GCN and $Cu(211_{)LV}$-5.5GCN.

2H → CHO + H → CHOH→CH + OH (see details in Figure S3).

On Cu(111)-7.5GCN, $Cu(111)_{CV}$-6.5GCN, $Cu(211)_{LV}$-5.5GCN, and $Cu(211)_{PV}$-4GCN, the dominant path is CO + 2H → CHO + H → CHOH→CH + OH. On $Cu(211)_{PV}$-4.7GCN, that is CO + H → CHO → CH + O. On $Cu(111)_{LV}$-5.5GCN, there are two competitive paths: CO + H → CHO → CH + O and CO + 2H → CHO + H → CHOH→CH + OH. The overall barriers of CH production are in the sequence $Cu(211)_{PV}$-4GCN > $Cu(111)_{LV}$-5.5GCN > $Cu(211)_{LV}$-5.5GCN ≈ $Cu(211)_{PV}$-4.7GCN > Cu(111)-7.5GCN ≈ $Cu(111)_{CV}$-6.5GCN (3.29, 2.90/2.91, 2.46, 2.44, 2.34, and 2.17 eV); thus, Cu(111)-7.5GCN and $Cu(111)_{CV}$-6.5GCN exhibit a higher catalytic activity toward CH production.

3.4.2. CH_2 Production. For CH_2 production, three paths, CO + H → CHO + H → CH_2O → CH_2 + O, CO + H → CHO + 2H → CHOH+H → CH_2OH → CH_2 + OH, and CO + H → CHO + 2H → CH_2O + H → CH_2OH → CH_2 + OH, are considered (see details in Figures S5 and S6). CO + H → CHO + 2H → CH_2O + H → CH_2OH → CH_2 + OH is the dominant path on $Cu(111)_{CV}$-6.5GCN, $Cu(111)_{LV}$-5.5GCN, $Cu(211)_{LV}$-5.5GCN, $Cu(211)_{PV}$-4.7GCN, and $Cu(211)_{PV}$-4GCN. However, Cu(111)-7.5GCN corresponds to the dominant path CHO + 2H → CHOH+H → CH_2OH → CH_2 + OH. The overall barrier of CH_2 production is in the sequence $Cu(211)_{PV}$-4GCN > Cu(111)-7.5GCN > $Cu(211)_{PV}$-4.7GCN > $Cu(111)_{LV}$-5.5GCN ≈ $Cu(111)_{CV}$-6.5GCN > $Cu(211)_{LV}$-5.5GCN (2.42, 2.03, 1.71, 1.52, 1.49, and 1.17 eV); thus, $Cu(211)_{LV}$-5.5GCN exhibits the highest activity toward CH_2 production.

3.4.3. CH_3 Production. The production of CH_3 primarily goes through the path CO + H → CHO + H → CH_2O + H → CH_3O → CH_3 + O on Cu(111)-7.5GCN, $Cu(111)_{CV}$-6.5GCN, $Cu(111)_{LV}$-5.5GCN, $Cu(211)_{LV}$-5.5GCN, $Cu(211)_{PV}$-4.7GCN, and $Cu(211)_{PV}$-4GCN, see Figures S7 and S8. The overall barriers of CH_3 production are in the sequence $Cu(111)_{LV}$-5.5GCN > Cu(111)-7.5GCN > $Cu(211)_{PV}$-4GCN > $Cu(111)_{CV}$-6.5GCN > $Cu(211)_{PV}$-4.7GCN ≈ $Cu(211)_{LV}$-5.5GCN (2.58, 2.51, 2.41, 1.75, 1.66, and 1.58 eV). Thus, both $Cu(211)_{PV}$-4.7GCN and $Cu(211)_{LV}$-5.5GCN have a much higher catalytic activity for CH_3 production compared to other Cu surfaces.

3.4.4. CH_3OH Production. CH_3OH could be generated through the hydrogenation of CH_3O and CH_2OH, see Figures S9 and S10; the dominant path is CHO + 3H → CH_2O + 2H → CH_3O + H → CH_3OH on Cu(111)-7.5GCN, $Cu(111)_{CV}$-6.5GCN, $Cu(211)_{LV}$-5.5GCN, $Cu(211)_{PV}$-4.7GCN, and $Cu(211)_{PV}$-4GCN. However, CHO + 3H → CH_2O + 2H → CH_2OH + H → CH_3OH dominantly contributes to CH_3OH production on $Cu(111)_{LV}$-5.5GCN. The overall barrier of CH_3OH production is in the sequence $Cu(211)_{PV}$-4GCN > Cu(111)-7.5GCN ≈ $Cu(211)_{LV}$-5.5GCN > $Cu(111)_{LV}$-5.5GCN > $Cu(211)_{PV}$-4.7GCN ≈ $Cu(111)_{CV}$-6.5GCN (2.20, 1.68, 1.58, 1.49, 1.27, and 1.23 eV); thus, $Cu(211)_{PV}$-4.7GCN

https://doi.org/10.1021/acs.jpcc.1c04763
J. Phys. Chem. C 2021, 125, 23085−23097

and $Cu(111)_{CV}$-6.5GCN are preferable for CH_3OH production.

3.5. General Discussion. *3.5.1. Relationship of Cu Active Site GCNs with the Existing Form of Primary CH_x Monomers.* The above results show that the GCNs of Cu active sites around the vacancy will influence the most favorable path of CH_x (x = 1−3) and CH_3OH production, as presented in Figure 6; starting from CO + H species, the overall barriers of

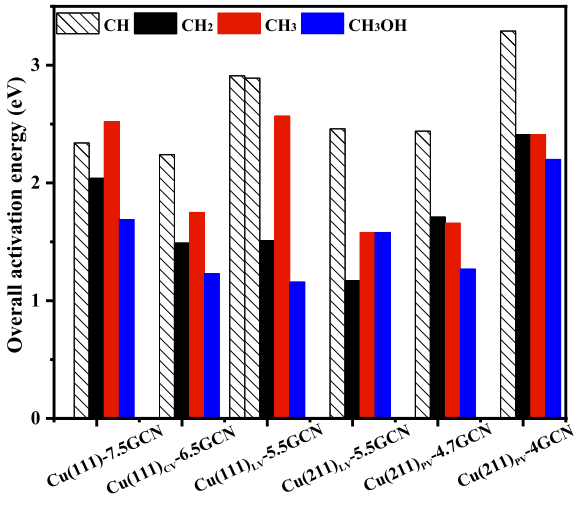

Figure 6. Overall activation energy for the optimal routes of CH_x (x = 1−3) and CH_3OH production with respect to CHO + H species on Cu(111)-7.5GCN, $Cu(111)_{CV}$-6.5GCN, $Cu(111)_{LV}$-5.5GCN, $Cu(211)_{LV}$-5.5GCN, $Cu(211)_{PV}$-4.7GCN, and $Cu(211)_{PV}$-4GCN. $Cu(111)_{LV}$-5.5GCN has two different overall activation energies for the optimal routes of CH production since two parallel paths exist for CH production.

CH, CH_2, and CH_3 production correspond to 2.34, 2.03, and 2.51 eV on Cu(111)-7.5GCN, and the primary CH_x monomer is CH_2, which is in agreement with the results reported for Cu(111).[1] Similarly, CH_2 is still the primary CH_x monomer on $Cu(111)_{CV}$-6.5GCN, $Cu(111)_{LV}$-5.5GCN, and $Cu(211)_{LV}$-5.5GCN;[19] the overall barriers are 1.49, 1.52, and 1.17 eV. However, the primary CH_x monomers are CH_2 and CH_3 on $Cu(211)_{PV}$-4.7GCN (1.71/1.66 eV) and $Cu(211)_{PV}$-4GCN (2.42/2.41 eV), respectively. These results indicate that the existing form of primary CH_x monomers on the Cu catalyst is closely linked to the GCNs of Cu active sites.

3.5.2. Relationship of the GCNs of Cu Active Sites with CH_x Production Activity. In order to further reveal the relationship of the GCNs of Cu active sites with the activity of CH_x (x = 1−3) production under the realistic reaction conditions (P_{CO} = 4 atm; P_{H2} = 8 atm; T = 523 K), the microkinetic modeling[2,61,63,64] has been implemented for syngas conversion to CH_x (x = 1−3) and CH_3OH on Cu(111)-7.5GCN, $Cu(111)_{CV}$-6.5GCN, $Cu(111)_{LV}$-5.5GCN, $Cu(211)_{LV}$-5.5GCN, $Cu(211)_{PV}$-4.7GCN, and $Cu(211)_{PV}$-4GCN to evaluate the production rate of CH_x (see details in the Supporting Information) in which the effects of surface species coverage, temperature, and pressure are considered, as listed in Tables S4 and S5.

As shown in Figure 7, the production rate of CH and CH_3 is slower than that of CH_2 on Cu(111)-7.5GCN, $Cu(111)_{CV}$-6.5GCN, $Cu(111)_{LV}$-5.5GCN, $Cu(211)_{LV}$-5.5GCN, $Cu(211)_{PV}$-4.7GCN, and $Cu(211)_{PV}$-4GCN; thus, CH_2 is the primary CH_x monomer. The rate (molecules·s^{-1}·$site^{-1}$) of

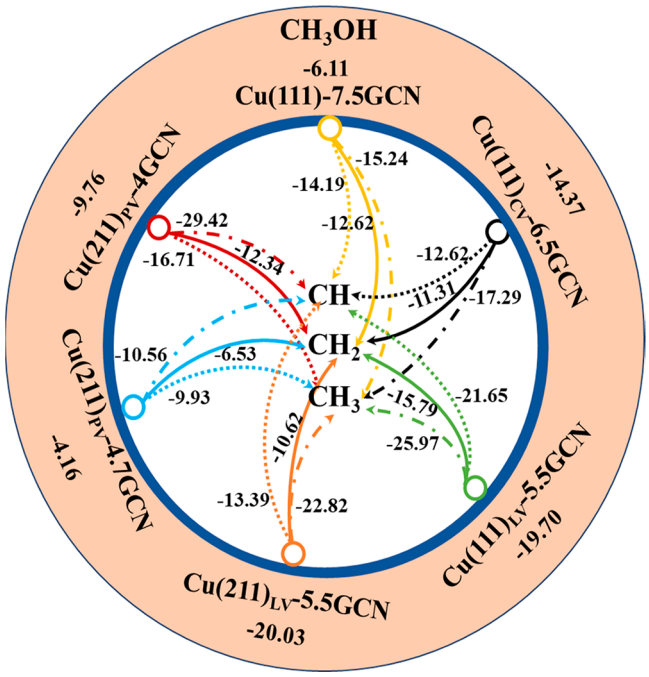

Figure 7. Rates (lgr/molecules·s^{-1}·$site^{-1}$) of CH_x (x = 1−3) and CH_3OH production at 523 K on Cu(111)-7.5GCN, $Cu(111)_{CV}$-6.5GCN, $Cu(111)_{LV}$-5.5GCN, $Cu(211)_{LV}$-5.5GCN, $Cu(211)_{PV}$-4.7GCN, and $Cu(211)_{PV}$-4GCN.

CH_2 production is in the sequence $Cu(211)_{PV}$-4.7GCN (1.37×10^{-6}) > $Cu(211)_{LV}$-5.5GCN (2.38×10^{-11}) > $Cu(111)_{CV}$-6.5GCN (4.94×10^{-12}) > $Cu(211)_{PV}$-4GCN (2.56×10^{-12}) ≈ Cu(111)-7.5GCN (2.41×10^{-13}) > $Cu(111)_{LV}$-5.5GCN (1.62×10^{-16}); especially, $Cu(211)_{PV}$-4.7GCN exhibits the highest catalytic activity toward CH_2 monomer production; thus, the GCNs of Cu active sites obviously affect the activity of CH_2 production.[51,52] Furthermore, both $Cu(111)_{LV}$-5.5GCN and $Cu(211)_{LV}$-5.5GCN have the same GCNs of Cu active sites; however, $Cu(211)_{LV}$-5.5GCN exhibits a higher activity than $Cu(111)_{LV}$-5.5GCN, which is in agreement with the DFT results.

3.5.3. Effect of Methanol on the Selectivity of CH_x. On Cu catalysts, CH_3OH is the dominant byproduct to reduce the yield and selectivity of CH_x. As shown in Figure 7, the rate (molecules·s^{-1}·$site^{-1}$) of CH_3OH production is larger than that of the primary CH_2 monomer on Cu(111)-7.5GCN, $Cu(211)_{PV}$-4.7GCN, and $Cu(211)_{PV}$-4GCN; correspondingly, CH_3OH selectivity is 100, 99.58, and 99.77% (Table S6), respectively; namely, Cu(111)-7.5GCN, $Cu(211)_{PV}$-4.7GCN, and $Cu(211)_{PV}$-4GCN present a higher activity and selectivity toward CH_3OH production. Conversely, on $Cu(111)_{CV}$-6.5GCN, $Cu(111)_{LV}$-5.5GCN, and $Cu(211)_{LV}$-5.5GCN, the rate of CH_2 production is larger than that of CH_3OH, and CH_2 selectivity is 95.24, 99.98, and 99.82%; namely, $Cu(111)_{CV}$-6.5GCN, $Cu(111)_{LV}$-5.5GCN, and $Cu(211)_{LV}$-5.5GCN exhibit a higher activity and selectivity toward CH_2 production, and the results on $Cu(111)_{CV}$-6.5GCN and $Cu(111)_{LV}$-5.5GCN are not consistent with DFT results, which is caused by the effects of surface species coverage and pressure. Among them, although $Cu(211)_{PV}$-4.7GCN performs the highest rate of CH_2 and CH_3OH production, the rate of CH_3OH production is more than two orders of magnitude faster than that of CH_2 production; namely, $Cu(211)_{PV}$-4.7GCN results in high CH_3OH selectivity. Meanwhile, $Cu(111)_{CV}$-6.5GCN,

https://doi.org/10.1021/acs.jpcc.1c04763
J. Phys. Chem. C 2021, 125, 23085−23097

$Cu(111)_{LV}$-5.5GCN, and $Cu(211)_{LV}$-5.5GCN mainly produce CH_2; however, the rate of CH_2 production on these three catalysts is still more than 7−10 orders lower than the rate of CH_3OH production on $Cu(211)_{PV}$-4.7GCN. Thus, both $Cu(211)_{LV}$-5.5GCN and Cu(111)-6.5GCN are the most appropriate catalyst with moderate activity and excellent selectivity of CH_2 production; especially, $Cu(211)_{LV}$-5.5GCN has the highest activity and selectivity.

The product selectivity is closely linked with reaction energy;[65−67] for example, Yang et al.[66] proposed that the difference between C_2H_4 hydrogenation barriers and its adsorption energies can be used to effectively evaluate C_2H_4 selectivity in C_2H_2 semihydrogenation; namely, the energy difference is the important driving force to alter product selectivity. Dang et al.[67] used the effective energy barrier difference between CH_2 + CH_2 coupling and CH_3 + CHO coupling as an energy descriptor to estimate product selectivity in syngas conversion. Interestingly, Kozuch et al.[68] found that the reaction effective barrier is not the barriers of the rate-determining steps, but the energy differences between two rate-determining states in the whole energy profiles, namely, the reaction effective barrier, correspond to the energy difference between the transition states with the highest energy and the most stable species in the reaction.

Thus, the effective barrier difference between the primary CH_x (x = 1−3) and CH_3OH production is compared to unravel the underlying factor to alter the selectivity of primary CH_x (x = 1−3) on the Cu catalyst. Hence, the effective barrier (E_a^{eff}) can be defined as the following equation:[67]

$$E_a^{eff} = E_{HTS} - E_{ADS} \quad (2)$$

where E_{HTS} represents the transition states with the highest energy, E_{ADS} represents the energy of the most stable intermediate, and the E_a^{eff} values for the primary CH_x (x = 1−3) and CH_3OH production are listed in Table S6. The E_a^{eff} value for the primary CH_x (x = 1−3) production is lower than that of CH_3OH production, which leads to the negative ΔE_a^{eff} value, as presented in Figure 8; on $Cu(111)_{LV}$-5.5GCN, $Cu(211)_{LV}$-5.5GCN, and $Cu(111)_{CV}$-6.5GCN, the greater negative value of ΔE_a^{eff} corresponds to the high selectivity of primary CH_x (x = 1−3). However, the smaller negative or even positive ΔE_a^{eff} corresponds to the low selectivity of primary CH_x (x = 1−3); namely, the greater negative value of ΔE_a^{eff} will promote CH_x (x = 1−3) production. Thus, ΔE_a^{eff} can be used as the significant driving force descriptor to alter product selectivity.

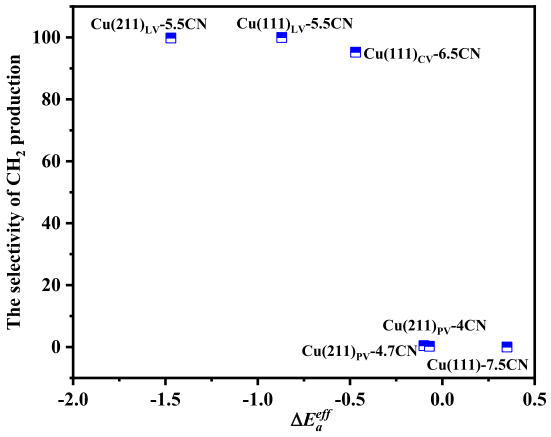

Figure 8. Relationship of ΔE_a^{eff} with the selectivity of the primary CH_x (x = 1−3) monomer production. ΔE_a^{eff} is the difference of effective barriers for CH_3OH and CH_2 production.

Furthermore, the above results show that Cu(111)-7.5GCN, $Cu(211)_{PV}$-4.7GCN, and $Cu(211)_{PV}$-4GCN dominantly contribute to CH_3OH production, while $Cu(111)_{CV}$-6.5GCN, $Cu(111)_{LV}$-5.5GCN, and $Cu(211)_{LV}$-5.5GCN are mainly responsible for primary CH_x (x = 1−3) monomer production. Thus, the further hydrogenation of the primary CH_x (x = 1−3) monomer may occur on $Cu(111)_{CV}$-6.5GCN, $Cu(111)_{LV}$-5.5GCN, and $Cu(211)_{LV}$-5.5GCN. Up to now, previous study results[18,20,61] show that the further hydrogenation of the primary CH_x (x = 1−3) monomer to CH_x (x = 2−4) is difficult to occur on the Cu catalysts with 6.7-GCN and 5.5-GCN Cu active sites. For example, Zhang et al.[18] calculated the production of C_2 oxygenates from syngas on Cu(110)-5.5GCN, indicating that CH_x (x = 2, 3) are the primary monomers, and CO insertion into CH_2 to CH_2CO is dominant compared to the hydrogenation of CH_x (x = 2, 3) to CH_x (x = 3, 4). DFT studies by Zhang et al.[20] showed that CH_3 is the primary CH_x (x = 1−3) monomer on Cu(211)-5.5GCN, and CHO insertion into CH_3 is kinetically favored compared to CH_3 hydrogenation to CH_4; namely, Cu(211)-5.5GCN is disadvantageous for the hydrogenation of CH_3 to CH_4. Sun et al.[61] found that CH_3 is the primary CH_x (x = 1−3) monomer on Cu(100)-6.7GCN, and CHO insertion into CH_3 to CH_3CHO is kinetically favored compared to the hydrogenation of CH_3 to CH_4. Based on the above analysis, the further hydrogenation of the primary CH_x (x = 1−3) monomer is difficult to occur on the Cu catalysts with 6.7-GCN and 5.5-GCN Cu active sites, so the further hydrogenation of the primary CH_x (x = 1−3) monomer on $Cu(111)_{CV}$-6.5GCN, $Cu(111)_{LV}$-5.5GCN, and $Cu(211)_{LV}$-5.5GCN is not considered in this study.

3.5.4. Electronic Properties. The catalyst surface with different GCNs could lead to the change of the active site structure and further impacts the electronic properties of the surface to perform different activities toward the target reaction.[69−71] In order to clarify the microscopic reason why the GCNs of Cu active sites affect the catalytic performance of the primary CH_2 monomer in syngas conversion, the electronic properties of Cu catalysts are calculated, and the relationship of the electronic properties with the catalytic performance is obtained.

The activity of transition metals is closely associated with their empty d-orbitals and/or d-electrons, and the average energy of the d-band center can be defined as eq 3:[72]

$$\varepsilon_d = \frac{\int_{-\infty}^{Ef} E\rho_d(E)d(E)}{\int_{-\infty}^{Ef} \rho_d(E)d(E)} \quad (3)$$

As shown in Figure 9, the degree of deviation between the d-band center and Fermi level is in the sequence $Cu(211)_{PV}$-4GCN (−2.46) > Cu(111)-7.5GCN (−2.45) = $Cu(111)_{CV}$-6.5GCN (−2.45) > $Cu(211)_{PV}$-4.7GCN (−2.42) > $Cu(111)_{LV}$-5.5GCN (−2.40) > $Cu(211)_{LV}$-5.5GCN (−2.32), suggesting that the catalyst surface with different CNs make the catalyst surface present different electronic properties. Then, the relationship of the d-band center of the Cu surface with the activity of CH_2 production is considered, and the d-band center of surface Cu atoms around the vacancy has a

https://doi.org/10.1021/acs.jpcc.1c04763
J. Phys. Chem. C 2021, 125, 23085−23097

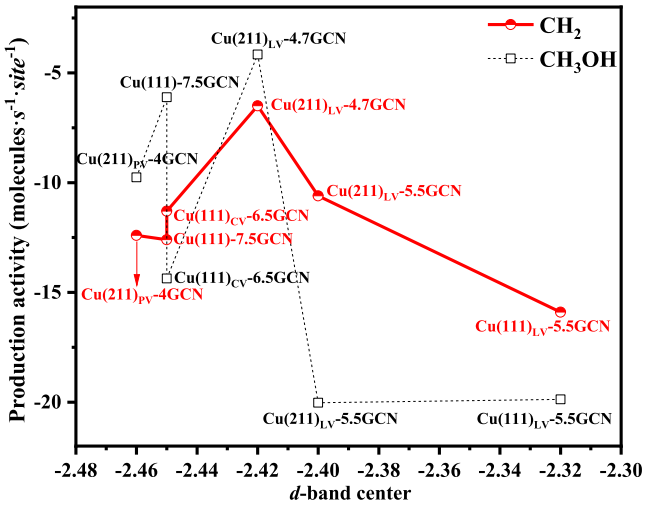

Figure 9. Volcano-shaped curve of CH_2 production activity as a function of surface *d*-band center of Cu atoms around the vacancy as denoted in the red line; the blank dotted line shows the trend of CH_3OH production activity with the increase of surface *d*-band centers of Cu atoms around the vacancy on Cu(111)-7.5GCN, $Cu(111)_{CV}$-6.5GCN, $Cu(111)_{LV}$-5.5GCN, $Cu(211)_{LV}$-5.5GCN, $Cu(211)_{PV}$-4.7GCN, and $Cu(211)_{PV}$-4GCN.

volcano-shaped curve with the activity of CH_2 production on Cu(111)-7.5GCN, $Cu(111)_{CV}$-6.5GCN, $Cu(111)_{LV}$-5.5GCN, $Cu(211)_{LV}$-5.5GCN, $Cu(211)_{PV}$-4.7GCN, and $Cu(211)_{PV}$-4GCN. Thus, there is a semiquantitative relationship between the GCNs of Cu active sites and the activity of CH_2 production. $Cu(211)_{PV}$-4.7GCN has the highest activity of CH_2 and CH_3OH production that is attributed to the moderate *d*-band center; however, $Cu(211)_{PV}$-4.7GCN exhibits a higher CH_3OH production activity instead of CH_2, leading to a low CH_2 selectivity. Overall, based on the literature and our calculated results, the relationship of GCNs with the activity of CH_x (x = 1−3) intermediate production offers the guide for the construction of realistic Cu catalysts with excellent catalytic performance for syngas conversion. On the other hand, similar results are also obtained for other reactions on the metal catalysts; for example, Lima et al.[73] found that the activity of the ORR on the Au(111), Ag(111), Pd(111), Rh(111), Ir(111), and Ru(0001) catalysts shows a volcano-shaped curve with the *d*-band center of the catalysts. Ando et al.[74] also revealed that the relationship between the activity of the ORR and *d*-band center of the surface Pt active site on the PtPb catalysts presents a volcano-shaped curve, and the moderate *d*-band center has the highest ORR activity.

Substantially, the *d*-band center of the catalyst impacts the adsorption ability of key intermediates[75,76] and further alters the catalytic activity. For example, Mavrikakis et al.[76] found that the lattice constant expansion of the Ru(0001) surface enhances CO chemisorption ability since the *d*-band center moves up in energy, which makes the Ru(0001) surface dramatically more reactive toward the dissociation of CO. Our results show that CH_2 is the primary CH_x monomer on Cu(111)-7.5GCN, $Cu(111)_{CV}$-6.5GCN, $Cu(111)_{LV}$-5.5GCN, $Cu(211)_{LV}$-5.5GCN, $Cu(211)_{PV}$-4.7GCN, and $Cu(211)_{PV}$-4GCN, and CH_2 is mainly produced via the C−O bond splitting of CH_2OH. Hence, the relationship of the *d*-band center of the Cu surface with the adsorption ability of CH_2OH is considered, as presented in Figure 3b; CH_2OH adsorption ability shows a U-shaped curve relationship with the GCN of the Cu active site; among them, CH_2OH adsorption ability is the greatest on $Cu(211)_{LV}$-5.5GCN and $Cu(211)_{PV}$-4.7GCN with the moderate *d*-band center compared to that on the other surfaces, so the C−O bond of CH_2OH is highly activated, resulting in the easier C−O bond cleavage of CH_2OH to exhibit high activity of CH_2 production. However, CH_2OH adsorption ability is lower on Cu(111)-7.5GCN, $Cu(111)_{CV}$-6.5GCN, $Cu(111)_{LV}$-5.5GCN, and $Cu(211)_{PV}$-4GCN with the *d*-band center either too far or too close from the Fermi level; thus, the C−O bond activation of CH_2OH is weaker, leading to the weaker activity of CH_2 production. Thus, taking Figure 3b and Figure 9 into consideration, it is concluded that the relationship of CH_x production with the *d*-band center of different Cu surfaces also shows a volcano-shaped curve.

As presented in Figure 10a−f, the differential charge density shows that on $Cu(111)_{PV}$-4.7GCN, the Cu atoms around the vacancy has moderate electron accumulation, which results in the excellent activity toward CH_2 production. However, Cu(111)-7.5GCN, $Cu(111)_{CV}$-6.5GCN, $Cu(111)_{LV}$-5.5GCN, and $Cu(211)_{LV}$-5.5GCN with more electron accumulation and $Cu(211)_{PV}$-4GCN with less electron accumulation reduced the activity of CH_2 production. Aiming at quantitatively analyzing the accepted electron number of Cu atoms around the vacancy, the average Mulliken charge (*e*) is calculated (Table S6), and the sequence is $Cu(111)_{CV}$-6.5GCN (0.017) > $Cu(111)_{LV}$-5.5GCN (0.015) > $Cu(211)_{LV}$-5.5GCN (0.011) >

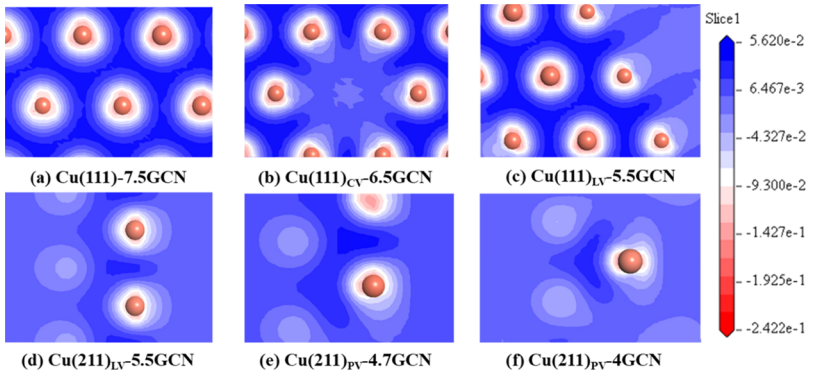

Figure 10. Differential charge density of surface Cu atoms around the vacancy on (a) Cu(111)-7.5GCN, (b) $Cu(111)_{CV}$-6.5GCN, (c) $Cu(111)_{LV}$-5.5GCN, (d) $Cu(211)_{LV}$-5.5GCN, (e) $Cu(211)_{PV}$-4.7GCN, and (f) $Cu(211)_{PV}$-4GCN. The blue and pink shaded regions represent the charge gain and charge loss, respectively.

https://doi.org/10.1021/acs.jpcc.1c04763
J. Phys. Chem. C 2021, 125, 23085−23097

Cu(111)-7.5GCN (0.008) > $Cu(211)_{PV}$-4.7GCN (0.003) > $Cu(211)_{PV}$-4GCN (−0.001), which is in agreement with the results by the differential charge density. $Cu(211)_{PV}$-4.7GCN with a moderate average charge (0.003) exhibits the highest activity of CH_2 production, and CH_2 activity is closely related to the average charge of Cu atoms around the active sites.

Thus, the GCNs of the Cu active site induced by the vacancies show a significant role in tuning the catalytic activity and selectivity of the primary CH_2 monomer (Figure 8). Moreover, the GCNs could change the most favorable path of CH_x (x = 1−3) and CH_3OH production and impact the existing form of primary CH_x (x = 1−3) monomers. A valuable structure clue for improving the activity and selectivity of CH_2 production is proposed; that is, the 6.5-GCN and 5.5-GCN of Cu active sites exhibit a higher CH_2 selectivity and moderate activity of CH_2 production. Thus, the greater catalytic performance toward syngas conversion to CH_x should focus on the 6.5- and 5.5-GCN Cu active sites on the Cu catalyst.

3.6. Comparisons with the Previous Theoretical and Experimental Results about the CN Effect of Active Sites on the Catalytic Performance. Extensive studies have presented the effects of CN on the catalytic performance. For example, Li et al.[77] theoretically found that the CN of single-atom Pt is necessary for adjusting the bonding strength of the O atom, and the 4.8-CN of the Pt active site has unique ORR performance. Torio et al.[78] studied the dissociation of CH_4 on the Pt(111), Pt(211), and Pt(110) with the 9-, 7-, and 7-CN of Pt active sites, suggesting that 7-CN of the Pt active site significantly enhances the activity of CH_4 dissociation. Moreover, Ren et al.[79] reported that with the increasing CNs of the Pt active site, the hydrogenation activity decreases significantly. However, DFT studies by Ouyang et al.[80] found that 9-CN of the Au active site shows distinct oxidative performance compared with 7-CN of the Au active site. Han et al.[81] reported that the Ru_3Cl_9, Ru_3Cl_7, Ru_5Cl_7, Ru_3Cl_3, and Ru_3 clusters show a decrease trend of CN; among them, Ru_5Cl_7 clusters exhibit the highest activity toward acetylene hydrochlorination. Wang et al.[72] studied toluene oxidation on the α-MnO_2 catalysts with 3-CN, 4-CN, and 5-CN of the Mn active site, and the Mn active site with 4-CN has positive effects on the activity of toluene oxidation.

The above reported experimental and theoretical studies showed that the moderate CN of active sites could show excellent catalytic activity. Furthermore, our studies found that from 4-GCN to 7.5-GCN of Cu active sites, the 4.7-GCN of the Cu active site exhibits the highest activity of CH_2 and CH_3OH production; however, it exhibits a low CH_2 selectivity. In addition, the moderate GCN of the Cu active site (GCN = 5.5 and 6.5) has moderate activity of CH_2 production and the highest selectivity of the CH_2 monomer instead of CH_3OH in syngas conversion.

4. CONCLUSIONS

In this study, the role of GCNs of the Cu active site in syngas-to-CH_x (x = 1−3) and CH_3OH is revealed using DFT calculations and microkinetic modeling. Cu(111)-7.5GCN, $Cu(111)_{PV}$-6.5GCN, $Cu(111)_{LV}$-5.5GCN, $Cu(211)_{LV}$-5.5GCN, $Cu(211)_{PV}$-4.7GCN, and $Cu(211)_{PV}$-4GCN are constructed to model Cu catalysts with different GCNs of Cu active sites and coordination environments. The activity and selectivity of CH_x (x = 1−3) and CH_3OH production on these Cu catalysts are analyzed. The obtained results show that the GCNs of the Cu active site can change the most favorable path and the existing form of the primary CH_x (x = 1−3) monomer. Specifically, the CH_2 monomer is the primary CH_x monomer on Cu(111)-7.5GCN, $Cu(111)_{PV}$-6.5GCN, $Cu(111)_{LV}$-5.5GCN, $Cu(211)_{LV}$-5.5GCN, $Cu(211)_{PV}$-4.7GCN, and $Cu(211)_{PV}$-4GCN; the 4.7-GCN of the Cu active site exhibits the highest activity of CH_2 and CH_3OH production; however, CH_3OH is the dominant product. The moderate GCN (GCN = 5.5 and 6.5) shows the excellent activity of CH_2 production and the highest CH_2 selectivity. However, the rate of CH_2 production on $Cu(111)_{CV}$-6.5GCN, $Cu(111)_{LV}$-5.5GCN, and $Cu(211)_{LV}$-5.5GCN is still far lower than the rate of CH_3OH production on $Cu(211)_{PV}$-4.7GCN. Moreover, the different catalytic activity on $Cu(111)_{LV}$-5.5GCN and $Cu(211)_{LV}$-5.5GCN is attributed to the different coordination environment. Furthermore, the analysis of electronic properties shows that the highest catalytic activity toward CH_2 production on the 4.7-GCN of the Cu active site is ascribed to the moderate d-band center and average Mulliken charge. Thus, adjusting the GCNs of the Cu active site is an effective way to construct Cu catalysts with an outstanding catalytic performance for the production of C_2 oxygenates from syngas, which has a wide influence on the development of the catalysts.

■ ASSOCIATED CONTENT

Supporting Information

The Supporting Information is available free of charge at https://pubs.acs.org/doi/10.1021/acs.jpcc.1c04763.

The computational details and supplementary date, including the generalized coordinate number (GCN), the methods of adsorption energy, the reactions involved in CO activation to CH_x and CH_3OH, and microkinetic modeling (PDF)

■ AUTHOR INFORMATION

Corresponding Authors

Baojun Wang − *State Key Laboratory of Clean and Efficient Coal Utilization, Taiyuan University of Technology, Taiyuan 030024 Shanxi, P.R. China; Key Laboratory of Coal Science and Technology, (Taiyuan University of Technology), Ministry of Education, Taiyuan 030024 Shanxi, P.R. China;* orcid.org/0000-0002-9069-6720; Email: wangbaojun@tyut.edu.cn, wbj@tyut.edu.cn

Riguang Zhang − *State Key Laboratory of Clean and Efficient Coal Utilization, Taiyuan University of Technology, Taiyuan 030024 Shanxi, P.R. China; Key Laboratory of Coal Science and Technology, (Taiyuan University of Technology), Ministry of Education, Taiyuan 030024 Shanxi, P.R. China;* orcid.org/0000-0001-8956-8425; Email: zhangriguang@tyut.edu.cn

Authors

Wantong Zhao − *State Key Laboratory of Clean and Efficient Coal Utilization, Taiyuan University of Technology, Taiyuan 030024 Shanxi, P.R. China; Key Laboratory of Coal Science and Technology, (Taiyuan University of Technology), Ministry of Education, Taiyuan 030024 Shanxi, P.R. China*

Lixuan Ma − *State Key Laboratory of Clean and Efficient Coal Utilization, Taiyuan University of Technology, Taiyuan 030024 Shanxi, P.R. China; Key Laboratory of Coal Science and Technology, (Taiyuan University of Technology), Ministry of Education, Taiyuan 030024 Shanxi, P.R. China*

https://doi.org/10.1021/acs.jpcc.1c04763
J. Phys. Chem. C 2021, 125, 23085−23097

Lixia Ling − *State Key Laboratory of Clean and Efficient Coal Utilization, Taiyuan University of Technology, Taiyuan 030024 Shanxi, P.R. China; Key Laboratory of Coal Science and Technology, (Taiyuan University of Technology), Ministry of Education, Taiyuan 030024 Shanxi, P.R. China*

Complete contact information is available at: https://pubs.acs.org/10.1021/acs.jpcc.1c04763

Notes

The authors declare no competing financial interest.

■ ACKNOWLEDGMENTS

This work was financially supported by Key Projects of National Natural Science Foundation of China (No. 21736007), the National Natural Science Foundation of China (Nos. 21776193, 22078221, and 21476155), and Top Young Innovative Talents of Shanxi.

■ REFERENCES

(1) Sun, X. C.; Zhang, R. G.; Wang, B. J. Insights into the Preference of CH_x(x=1-3) Formation from CO Hydrogenation on Cu(111) Surface. *Appl. Surf. Sci.* **2013**, *265*, 720−730.

(2) Ao, M.; Pham, G. H.; Sunarso, J.; Tade, M. O.; Liu, S. M. Active Centers of Catalysts for Higher Alcohol Synthesis from Syngas: A Review. *ACS Catal.* **2018**, *8*, 7025−7050.

(3) Spivey, J. J.; Egbebi, A. Heterogeneous Catalytic Synthesis of Ethanol from Biomass-derived Syngas. *Chem. Soc. Rev.* **2007**, *36*, 1514−1528.

(4) Medford, A. J.; Lausche, A. C.; Abild-Pedersen, F.; Temel, B.; Schjødt, N. C.; Nørskov, J. K.; Studt, F. Activity and Selectivity Trends in Synthesis Gas Conversion to Higher Alcohols. *Top. Catal.* **2014**, *57*, 135−142.

(5) Choi, Y. M.; Liu, P. Mechanism of Ethanol Synthesis from Syngas on Rh(111). *J. Am. Chem. Soc.* **2009**, *131*, 13054−13061.

(6) Wang, J. C.; Liu, Z. X.; Zhang, R. G.; Wang, B. J. Ethanol Synthesis from Syngas on the Stepped Rh(211) Surface: Effect of Surface Structure and Composition. *J. Phys. Chem. C* **2014**, *118*, 22691−22701.

(7) Mei, D. H.; Rousseau, R.; Kathmann, S. M.; Glezakou, V. A.; Engelhard, M. H.; Jiang, W. L.; Wang, C. M.; Gerber, M. A.; White, J. F.; Stevens, D. J. Ethanol Synthesis from Syngas over Rh-based/SiO_2 Catalysts: A Combined Experimental and Theoretical Modeling Study. *J. Catal.* **2010**, *271*, 325−342.

(8) Sheerin, E.; Reddy, G. K.; Smirniotis, P. Evaluation of Rh/$Ce_xTi_{1-x}O_2$ Catalysts for Synthesis of Oxygenates from Syngas Using XPS and TPR Techniques. *Catal. Today* **2016**, *263*, 75−83.

(9) Behrens, M.; Studt, F.; Kasatkin, I.; Kuhl, S.; Havecker, M.; Abild-Pedersen, F.; Zander, S.; Girgsdies, F.; Kurr, P.; Kniep, B. L.; Tovar, M.; Fischer, R. W.; Norskov, J. K.; Schlogl, R. The Active Site of Methanol Synthesis over Cu/ZnO/Al_2O_3. *Science* **2012**, *336*, 893−897.

(10) Kattel, S.; Ramírez, P. J.; Chen, J. G.; Rodriguez, J. A.; Liu, P. Active Sites for CO_2 Hydrogenation to Methanol on Cu/ZnO Catalysts. *Science* **2017**, *355*, 1296−1299.

(11) Grabow, L. C.; Mavrikakis, M. Mechanism of Methanol Synthesis on Cu through CO_2 and CO Hydrogenation. *ACS Catal.* **2011**, *1*, 365−384.

(12) Zhao, N.; Xu, R.; Wei, W.; Sun, Y. Cu/Mn/ZrO_2 Catalyst for Alcohol Synthesis by Fischer-Tropsch Modified Elements. *React. Kinet. Catal. Lett.* **2002**, *75*, 297−304.

(13) Xu, R.; Wei, W.; Li, W. H.; Hu, T. D.; Sun, Y. H. Fe Modified $CuMnZrO_2$ Catalysts for Higher Alcohols Synthesis from Syngas: Effect of Calcination Temperature. *J. Mol. Catal. A-Chem.* **2005**, *234*, 75−83.

(14) Ren, B. H.; Dong, X. Q.; Yu, Y. Z.; Wen, G. B.; Zhang, M. H. A Density Functional Theory Study on the Carbon Chain Growth of Ethanol Formation on Cu-Co (111) and (211) Surfaces. *Appl. Surf. Sci.* **2017**, *412*, 374−384.

(15) Li, T.; Wen, X. D.; Li, Y. W.; Jiao, H. J. Mechanistic Insight into CO Activation, Methanation and C-C Bond Formation from Coverage Dependent CO Hydrogenation on Fe(110). *Surf. Sci.* **2019**, *689*, No. 121456.

(16) Xu, M. T.; Iglesia, E. Carbon-Carbon Bond Formation Pathways in CO Hydrogenation to Higher Alcohols. *J. Catal.* **1999**, *188*, 125−131.

(17) Xiao, K.; Qi, X. Z.; Bao, Z. H.; Wang, X. X.; Zhong, L. S.; Fang, K. G.; Lin, M. G.; Sun, Y. H. CuFe, CuCo and CuNi Nanoparticles as Catalysts for Higher Alcohol Synthesis from Syngas: A Comparative Study. *Cat. Sci. Technol.* **2013**, *3*, 1591−1602.

(18) Zhang, R. G.; Sun, X. C.; Wang, B. J. Insight into the Preference Mechanism of CH_x(x=1-3) and C-C Chain Formation Involved in C_2 Oxygenate Formation from Syngas on the Cu(110) Surface. *J. Phys. Chem. C* **2013**, *117*, 6594−6606.

(19) Wei, C.; Zhang, R. G.; Ling, L. X.; Li, D. B.; Hou, B.; Wang, B. J. Syngas-to-C_2 Oxygenates on Cu-based Catalyst: Quantitative Insight into the Balancing Effect of Active $Cu^{\delta+}$($0\leq\delta\leq1$) Sites. *Chem. Eng. Sci.* **2020**, *224*, No. 115785.

(20) Zhang, R. G.; Wang, G. R.; Wang, B. J. Insights into the Mechanism of Ethanol Formation from Syngas on Cu and an Expanded Prediction of Improved Cu-based Catalyst. *J. Catal.* **2013**, *305*, 238−255.

(21) Fu, Q.; Bao, X. H. Confined Microenvironment for Catalysis Control. *Nat. Catal.* **2019**, *2*, 834−836.

(22) Schumann, J. L.; Medford, A. J.; Yoo, J. S.; Zhao, Z. J.; Bothra, P.; Cao, A.; Studt, F.; Abild-Pedersen, F.; Nørskov, J. K. Selectivity of Synthesis Gas Conversion to C_{2+} Oxygenates on fcc(111) Transition-Metal Surfaces. *ACS Catal.* **2018**, *8*, 3447−3453.

(23) Studt, F.; Behrens, M.; Kunkes, E. L.; Thomas, N.; Zander, S.; Tarasov, A.; Schumann, J.; Frei, E.; Varley, J. B.; Abild-Pedersen, F.; Nørskov, J. K.; Schlögl, R. The Mechanism of CO and CO_2 Hydrogenation to Methanol over Cu-Based Catalysts. *ChemCatChem* **2015**, *7*, 1105−1111.

(24) Liu, C. C.; He, Y.; Wei, L.; Zhang, Y. H.; Zhao, Y. X.; Hong, J. P.; Chen, S. F.; Wang, L.; Li, J. L. Hydrothermal Carbon-Coated TiO_2 as Support for Co-based Catalyst in Fischer−Tropsch Synthesis. *ACS Catal.* **2018**, *8*, 1591−1600.

(25) Luo, D.; Ren, P. J.; Liu, X. C.; Gao, R.; Zhou, Y. W.; Guo, W. P.; Yang, Y.; Li, Y. W.; Wen, X. D. Tailoring the Electronic Structure and Chemical Activity of Iron via Confining into Two Dimensional Materials. *J. Phys. Chem. C* **2018**, *122*, 24037−24045.

(26) Pan, X. L.; Bao, X. H. Reactions over Catalysts Confined in Carbon Nanotubes. *Chem. Commun.* **2008**, *47*, 6271−6281.

(27) Lu, P.; Chen, Q. J.; Yang, G. H.; Tan, L.; Feng, X. B.; Yao, J.; Yoneyama, Y.; Tsubaki, N. Space-confined Self-regulation Mechanism from a Capsule Catalyst to Realize an Ethanol Direct Synthesis Strategy. *ACS Catal.* **2020**, *10*, 1366−1374.

(28) Shun, H.; Wei, W.; Zheng, S.; Li, G. Z.; Kang, J.; Liu, Z. M.; Wang, G. C.; Zhang, Q. H.; Wang, Y. Carbon Nanotube-supported Bimetallic Cu-Fe Catalysts for Syngas Conversion to Higher Alcohols. *Mol. Catal.* **2019**, *479*, 151−163.

(29) Xiao, J. P.; Pan, X. L.; Guo, S. L.; Ren, P. J.; Bao, X. H. Toward Fundamentals of Confined Catalysis in Carbon Nanotubes. *J. Am. Chem. Soc.* **2015**, *137*, 477−482.

(30) Gao, G. P.; Bottle, S.; Du, A. J. Understanding the Activity and Selectivity of Single Atom Catalysts for Hydrogen and Oxygen Evolution via Ab Initial Study. *Cat. Sci. Technol.* **2018**, *8*, 996−1001.

(31) Jiang, L. Z.; Liu, K. L.; Hung, S. F.; Zhou, L. Y.; Qin, R. X.; Zhang, Q. H.; Liu, P. X.; Gu, L.; Chen, H. M.; Fu, G.; Zheng, N. Facet Engineering Accelerates Spillover Hydrogenation on Highly Diluted Metal Nanocatalysts. *Nat. Nanotechnol.* **2020**, *15*, 848−853.

(32) Xu, Y.; Chu, M. Y.; Liu, F. F.; Wang, X. C.; Liu, Y.; Cao, M. H.; Gong, J.; Luo, J.; Lin, H. P.; Li, Y. Y.; Zhang, Q. Revealing the Correlation between Catalytic Selectivity and the Local Coordination Environment of Pt Single Atom. *Nano Lett.* **2020**, *20*, 6865−6872.

(33) Xie, J. F.; Yang, X. Y.; Xie, Y. Defect Engineering in Two-dimensional Electrocatalysts for Hydrogen Evolution. *Nanoscale* **2020**, *12*, 4283−4294.
(34) Kopač, D.; Likozar, B.; Huš, M. Catalysis of Material Surface Defects: Multiscale Modeling of Methanol Synthesis by CO_2 Reduction on Copper. *Appl. Surf. Sci.* **2019**, *497*, No. 143783.
(35) Chen, Z. W.; Gao, W.; Zheng, W. T.; Jiang, Q. Steric Hindrance in Sulfur Vacancy of Monolayer MoS_2 Boosts Electrochemical Reduction of Carbon Monoxide to Methane. *ChemSusChem* **2018**, *11*, 1455−1459.
(36) Ali, S.; Liu, T. F.; Lian, Z.; Su, D. S.; Li, B. The Stability and Reactivity of Transition Metal Atoms Supported Mono and Divacancies Defected Carbon Based Materials Revealed from First Principles Study. *Appl. Surf. Sci.* **2019**, *473*, 777−784.
(37) Zhuang, T. T.; Liang, Z. Q.; Seifitokaldani, A.; Li, Y.; de Luna, P.; Burdyny, T.; Che, F. L.; Meng, F.; Min, Y. M.; Quintero-Bermudez, R.; Dinh, C. T.; Pang, Y.; Zhong, M.; Zhang, B.; Li, J.; Chen, P. N.; Zheng, X. L.; Liang, H.; Ge, W. N.; Ye, B. J.; Sinton, D.; Yu, S. H.; Sargent, E. H. Steering Post-C-C Coupling Selectivity Enables High Efficiency Electroreduction of Carbon Dioxide to Multicarbon Alcohols. *Nat. Catal.* **2018**, *1*, 421−428.
(38) Gu, Z. X.; Shen, H.; Chen, Z.; Yang, Y. Y.; Yang, C.; Ji, Y. L.; Wang, Y. H.; Zhu, C.; Liu, J. L.; Li, J.; Sham, T. K.; Xu, X.; Zheng, G. Efficient Electrocatalytic CO_2 Reduction to C_{2+} Alcohols at Defect-Site-Rich Cu Surface. *Aust. Dent. J.* **2021**, *5*, 429−440.
(39) Rong, X.; Wang, H. J.; Lu, X. L.; Si, R.; Lu, T. B. Controlled Synthesis of a Vacancy-Defect Single-Atom Catalyst for Boosting CO_2 Electroreduction. *Angew. Chem. Int. Ed.* **2020**, *132*, 1977−1981.
(40) Delley, B. An All-electron Numerical Method for Solving the Local Density Functional for Polyatomic Molecules. *J. Chem. Phys.* **1990**, *92*, 508.
(41) Perdew, J. P.; Burke, K.; Ernzerhof, M. Generalized Gradient Approximation Made Simple. *Phys. Rev. Lett.* **1996**, *77*, 3865−3868.
(42) Dolg, M.; Wedig, U.; Stoll, H.; Preuss, H. Energy-adjusted Ab Initio Pseudopotentials for the First Row Transition Elements. *J. Chem. Phys.* **1987**, *86*, 866.
(43) Hohenberg, P.; Kohn, W. Inhomogeneous Electron Gas. *Phys. Rev. B* **1964**, *136*, B864−B871.
(44) Zhou, C. G.; Wu, J. P.; Nie, A.; Forrey, R. C.; Tachibana, A.; Cheng, H. S. On the Sequential Hydrogen Dissociative Chemisorption on Small Platinum Clusters: A Density Functional Theory Study. *J. Phys. Chem. C* **2007**, *111*, 12773−12778.
(45) Bergner, A.; Dolg, M.; Kuchle, W.; Stoll, H.; Preuß, H. Ab Initio Energy-adjusted Pseudopotentials for Elements of Groups. *Mol. Phys.* **1993**, *80*, 1431−1441.
(46) Monkhorst, H. J.; Pack, J. D. Special Points for Brillonin-zone Integrations. *Phys. Rev. B* **1976**, *13*, 5188−5192.
(47) Govind, N.; Petersen, M.; Fitzgerald, G.; King-Smith, D.; Andzelm, J. A Generalized Synchronous Transit Method for Transition State Location. *Comput. Mater. Sci.* **2003**, *28*, 250−258.
(48) Halgren, T. A.; Lipscomb, W. N. The Synchronous-transit Method for Determining Reaction Pathways and Locating Molecular Transition States. *Chem. Phys. Lett.* **1977**, *49*, 225−232.
(49) Bengaarda, H. S.; Nørskova, J. K.; Sehested, J.; Clausen, B. S.; Nielsen, L. P.; Molenbroek, A. M.; Rostrup-Nielsen, J. R. Steam Reforming and Graphite Formation on Ni Catalysts. *J. Catal.* **2002**, *209*, 365−384.
(50) Lin, S.; Ma, J. Y.; Zhou, L. S.; Huang, C. J.; Xie, D. Q.; Guo, H. Influence of Step Defects on Methanol Decomposition: Periodic Density Functional Studies on Pd(211) and Kinetic Monte Carlo Simulations. *J. Phys. Chem. C* **2013**, *117*, 451−459.
(51) Gao, X. M.; Wang, S. J.; Lin, S. Defective Hexagonal Boron Nitride Nanosheet on Ni(111) and Cu(111): Stability, Electronic Structures, and Potential Applications. *ACS Appl. Mater. Interfaces* **2016**, *8*, 24238−24247.
(52) Xiang, K. S.; Zhu, F. F.; Liu, Y. C.; Pan, Y. F.; Wang, X. Y.; Yan, X.; Liu, H. A Strategy to Eliminate Carbon Deposition on a Copper Electrode in order to Enhance its Stability in CO_2RR Catalysis by Introducing Crystal Defects. *Electrochem. Commun.* **2019**, *102*, 72−77.
(53) Grunwaldt, J. D.; Molenbroek, A. M.; Topsøe, N. Y.; Topsøe, H.; Clausen, B. S. In Situ Investigations of Structural Changes in Cu/ZnO Catalysts. *J. Catal.* **2000**, *194*, 452−460.
(54) Kuld, S.; Thorhauge, M.; Falsig, H.; Elkjær, C. F.; Helveg, S.; Chorkendorff, I.; Sehested, J. Quantifying the Promotion of Cu Catalysts by ZnO for Methanol Synthesis. *Science* **2016**, *352*, 969−974.
(55) Calle-Vallejo, F.; Martinez, J. I.; GarcIa-Lastra, J. M.; Sautet, P.; Loffreda, D. Fast Prediction of Adsorption Properties for Platinum Nanocatalysts with Generalized Coordination Numbers. *Angew. Chem. Int. Ed.* **2014**, *126*, 8316−8319.
(56) Calle-Vallejo, F.; Loffreda, D.; Koper, M. T. M.; Sautet, P. Introducing Structural Sensitivity into Adsorption-energy Scaling Relations by Means of Coordination Numbers. *Nat. Chem.* **2015**, *7*, 403−410.
(57) Calle-Vallejo, F.; Tymoczko, J.; Colic, V.; Vu, Q. H.; Pohl, M. D.; Morgenstern, K.; Loffreda, D.; Sautet, P.; Schuhmann, W.; Bandarenka, A. S. Finding Optimal Surface Sites on Heterogeneous Catalysts by Counting Nearest Neighbors. *Science* **2015**, *350*, 185−189.
(58) Zhao, Z. L.; Chen, Z. Z.; Zhang, X.; Lu, G. Generalized Surface Coordination Number as an Activity Descriptor for CO_2 Reduction on Cu Surfaces. *J. Phys. Chem. C* **2016**, *120*, 28125−28130.
(59) Zhang, R. G.; Liu, F.; Wang, B. J. Co-decorated Cu Alloy Catalyst for C_2 Oxygenate and Ethanol Formation from Syngas on Cu-based Catalyst: Insight into the Role of Co and Cu as well as the Improved Selectivity. *Cat. Sci. Technol.* **2016**, *6*, 8036−8054.
(60) Yang, M. M.; Bao, X. H.; Li, W. X. Density Functional Theory Study of CH_x (x=1−3) Adsorption on Clean and CO Precovered Rh(111) Surfaces. *J. Chem. Phys.* **2007**, *127*, No. 024705.
(61) Sun, X. Y.; Yu, Y. Z.; Zhang, M. H. Insight into the Effect of Promoter Co on C_2 Oxygenate Formation from Syngas on CoCu(100) and Cu(100): A Comparative DFT Study. *Appl. Surf. Sci.* **2018**, *434*, 28−39.
(62) Luk, H. T.; Mondelli, C.; Ferre, D. C.; Stewart, J. A.; Perez-Ramirez, J. Status and Prospects in Higher Alcohols Synthesis from Syngas. *Chem. Soc. Rev.* **2017**, *46*, 1358−1426.
(63) Tafreshi, S. S.; Roldan, A.; de Leeuw, N. H. A Density Functional Theory Study of the Adsorption of Hydrazine on the Perfect and Defective Copper (100), (110) and (111) Surfaces. *J. Phys. Chem. C* **2014**, *45*, 26103−26114.
(64) Shetty, S.; Santen, R. A. V.; Stevens, P. A.; Raman, S. Molecular Steps for the Syngas Conversion on the Rh_6 Cluster. *J. Mol. Catal. A-Chem.* **2010**, *330*, 73−87.
(65) Kozuch, S.; Martin, J. M. L. What Makes for a Bad Catalytic Cycle? A Theoretical Study on the Suzuki-Miyaura Reaction within the Energetic Span Model. *ACS Catal.* **2011**, *1*, 246−253.
(66) Yang, B.; Burch, R.; Hardacre, C.; Headdock, G.; Hu, P. Origin of the Increase of Activity and Selectivity of Nickel Doped by Au, Ag, and Cu for Acetylene Hydrogenation. *ACS Catal.* **2012**, *2*, 1027−1032.
(67) Dang, Y.; Li, S. G. Catalytic Mechanism and Selectivity Prediction for Syngas Conversion over Pure and K-promoted Mo_2C Catalysts. *Appl. Catal. A-Gen.* **2021**, *610*, No. 117945.
(68) Kozuch, S.; Shaik, S. A Combined Kinetic-Quantum Mechanical Model for Assessment of Catalytic Cycles: Application to Cross-Coupling and Heck Reactions. *J. Am. Chem. Soc.* **2006**, *128*, 3355−3365.
(69) Raybaud, P.; Hafner, J.; Kresse, G.; Kasztelan, S.; Toulhoat, H. Structure, Energetics, and Electronic Properties of the Surface of a Promoted MoS_2 Catalyst: An Ab Initio Local Density Functional Study. *J. Catal.* **2000**, *190*, 128−143.
(70) Wang, Y. Y.; Xie, C.; Zhang, Z. Y.; Liu, D. D.; Chen, R.; Wang, S. Y. In Situ Exfoliated, N-Doped, and Edge-Rich Ultrathin Layered Double Hydroxides Nanosheets for Oxygen Evolution Reaction. *Adv. Funct. Mater.* **2018**, *28*, No. 1703363.
(71) Ma, X. F.; Xin, H. L. Orbitalwise Coordination Number for Predicting Adsorption Properties of Metal Nanocatalysts. *Phys. Rev. Lett.* **2017**, *118*, No. 036101.

(72) Wang, F.; Deng, J.; Impeng, S.; Shen, Y. J.; Yan, T. T.; Chen, G. R.; Shi, L. Y.; Zhang, D. S. Unraveling the Effects of the Coordination Number of Mn over α-MnO_2 Catalysts for Toluene Oxidation. *Chem. Eng. J.* **2020**, *396*, No. 125192.
(73) Lima, F. H. B.; Zhang, J.; Shao, M. H.; Sasaki, K.; Vukmirovic, M. B.; Ticianelli, E. A.; Adzic, R. R. Catalytic Activity-*d*-band Center Correlation for the O_2 Reduction Reaction on Platinum in Alkaline Solutions. *J. Phys. Chem. C* **2007**, *111*, 404−410.
(74) Ando, F.; Tanabe, T.; Gunji, T.; Kaneko, S.; Takeda, T.; Ohsaka, T.; Matsumoto, F. Effect of the *d* band Center on the Oxygen Reduction Reaction Activity of Electrochemically Dealloyed Ordered Intermetallic Platinum-Lead (PtPb) Nanoparticles Supported on TiO_2 Deposited Cup-stacked Carbon Nanotubes. *ACS Appl. Nano Mater.* **2018**, *1*, 2844−2850.
(75) Xin, H. L.; Vojvodic, A.; Voss, J.; Nørskov, J. K.; Abild-Pedersen, F. Effects of *d*-band Shape on the Surface Reactivity of Transition-metal Alloys. *Phys. Rev. B* **2014**, *89*, No. 115114.
(76) Mavrikakis, M.; Hammer, B.; Nørskov, J. K. Effect of Strain on the Reactivity of Metal Surfaces. *Phys. Rev. Lett.* **1998**, *81*, 2819−2822.
(77) Li, S. W.; Liu, J. J.; Yin, Z.; Ren, P. J.; Lin, L. L.; Gong, Y.; Yang, C.; Zheng, X. S.; Cao, R. C.; Yao, S. Y.; Deng, Y.; Liu, X.; Gu, L.; Zhou, W.; Zhu, J.; Wen, X.; Xu, B.; Ma, D. Impact of the Coordination Environment on Atomically Dispersed Pt Catalysts for Oxygen Reduction Reaction. *ACS Catal.* **2020**, *10*, 907−913.
(78) Torio, M. E.; Busnengo, H. F. Site-specific Product-selectivity of Stepped Pt Surfaces for Methane Dehydrogenation. *J. Phys. Chem. C* **2020**, *124*, 19649−19654.
(79) Ren, Y. J.; Tang, Y.; Zhang, L. L.; Liu, X. Y.; Li, L.; Miao, S.; Su, D. S.; Wang, A. Q.; Li, J.; Zhang, T. Unraveling the Coordination Structure-performance Relationship in Pt_1/Fe_2O_3 Single-atom Catalyst. *Nat. Commun.* **2019**, *10*, 4500.
(80) Ouyang, G.; Zhu, K. J.; Zhang, L.; Cui, P. F.; Teng, B. T.; Wen, X. D. Effects of Coordination Number of Au Catalyst on Oxygen Species and Their Catalytic Roles. *Appl. Surf. Sci.* **2016**, *387*, 875−881.
(81) Han, Y.; Sun, M. X.; Li, W.; Zhang, J. L. Influence of Chlorine Coordination Number on the Catalytic Mechanism of Ruthenium Chloride Catalysts in the Acetylene Hydrochlorination Reaction: A DFT Study. *Phys. Chem. Chem. Phys.* **2015**, *17*, 7720−7730.

https://doi.org/10.1021/acs.jpcc.1c04763
J. Phys. Chem. C 2021, 125, 23085−23097